catalysts

MDPI

Article

Nitrogen and Cobalt Co-Coped Carbon Materials Derived from Biomass Chitin as High-Performance Electrocatalyst for Aluminum-Air Batteries

Mi Wang [1], Jian Ma [2], Haoqi Yang [2], Guolong Lu [2,*], Shuchen Yang [1,*] and Zhiyong Chang [2]

[1] Engineering College, Changchun Normal University, Changchun, Jilin Province 130022, China; wangmi3214@126.com

[2] Key Laboratory of Bionic Engineering (Ministry of Education), College of Biological and Agricultural Engineering, Jilin University, Changchun, Jilin Province 130022, China; majian@126.com (J.M.); yhq1214@126.com (H.Y.); chanzhiyong@126.com (Z.C.)

* Correspondence: Guolonglu@jlu.edu.cn (G.L.); Ysc2017@mail.cncnc.edu.cn (S.Y.)

Received: 21 October 2019; Accepted: 10 November 2019; Published: 14 November 2019

Abstract: Development of convenient, economic electrocatalysts for oxygen reduction reaction (ORR) in alkaline medium is of great significance to practical applications of aluminum-air batteries. Herein, a biomass chitin-derived carbon material with high ORR activities has been prepared and applied as electrocatalysts in Al-air batteries. The obtained cobalt, nitrogen co-doped carbon material (CoNC) exhibits the positive onset potential 0.86 V vs. RHE (reversible hydrogen electrode) and high-limiting current density 5.94 mA cm^{-2}. Additionally, the durability of the CoNC material in alkaline electrolyte shows better stability when compared to the commercial Pt/C catalyst. Furthermore, the Al-air battery using CoNC as an air cathode catalyst provides the power density of 32.24 mW cm^{-2} and remains the constant discharge voltage of 1.17 V at 20 mA cm^{-2}. This work not only provides a facile method to synthesize low-cost and efficient ORR electrocatalysts for Al-air batteries, but also paves a new way to explore and utilize high-valued biomass materials.

Keywords: electrocatalyst; oxygen reduction reaction; Al-air battery; biomass; nitrogen-doped carbon

1. Introduction

Environmental deterioration and the depletion of finite resources stimulate research to seek and develop clean energy storage and conversion devices for the future. Metal (Al, Li, Zn, etc.)-air batteries [1–3] are considered the most promising candidates to replace the current fossil fuels due to their low carbon emissions, high theoretical specific capacity and energy density, etc. Among the batteries listed above, the Al-air battery is most abundant in the Earth's crust and possesses a high energy density (8.10 Wh g^{-1}) [4], which gives the Al-air battery considerable potential to be widely used; however, its poor electrochemical performance constrains its practical application.

Oxygen reduction reaction (ORR) is a key reaction affecting the discharged performance of energy storage devices such as fuel cells and metal-air batteries [5–7]. In order to enhance the discharged performance of these devices, a platinum-based electrocatalyst is commonly applied to overcome the sluggish ORR kinetics and accelerate the reaction process [8–11]. Despite the fact that platinum (Pt)-based catalysts are considered the most efficient ORR electrocatalyst, their expensive price and poor durability has limited their practical application [12–14]. Thus, great efforts have been devoted to exploring low-cost and high-performance carbon-based electrocatalysts. Among various carbon materials, graphene [15], carbon nanotubes (CNTs) [16] and activated carbon [17] are most frequently used in the preparation of carbon-based electrocatalysts due to their excellent physical and chemical properties. Although these carbon materials have shown remarkable catalytic activity, their cost still

limits their application. Therefore, it is important to seek another substitute for synthesizing a low-cost, carbon-based ORR electrocatalyst.

Biomass materials are the ideal carbon precursor for synthesizing ORR catalysts due to their renewability and large-scale and low-cost production [18–25]. Recently, several studies reported biomass-derived ORR catalysts with efficient catalytic activities. Li and co-workers [26] reported a low-cost method for transforming woody biomass into a single-atom, dispersed ORR catalyst. Wu et al. [27] synthesized kelp-derived, multilayer-graphene-encapsulated cobalt nanoparticles, which could possess efficient and stable electrocatalytic properties. Wei et al. [28] reported a reed-stalk-based Si-Fe/N/C ORR catalyst inspired by the Si-promoting graphitization findings. Deng et al. [29] described an activated carbon sheet derived from chitin, which was an efficient non-metal bifunctional electrocatalyst for both ORR and oxygen evolution reaction (OER). Li et al. [30] designed three-dimensional, honeycomb-like, nitrogen-doped carbon nanosheet/graphene nanonetwork films, which were prepared by dissolution and coagulation of chitin and graphene oxide in NaOH/urea aqueous solution using a repeated freezing–thawing process. Deng et al. [31] reported a chitin-derived porous carbon loaded with Co, N, and S heteroatoms, which showed excellent performance towards ORR, OER, and hydrogen evolution reaction (HER).

As numerous works reported, synthesizing non-precious ORR catalysts with high catalytic activity often requires further treatments such as activation [32] or hydrothermal [33] and chemical vaporous deposition [34]. However, intricate production steps are unpractical in industry and cannot achieve mass production. Herein, a one-step pyrolysis method was developed for preparation of a Co and N co-doped biocarbon catalyst derived from chitin. The obtained biomass, carbon-based material exhibits high catalytic activity and superior durability, which is comparable with the state-of-the-art noble-metal catalyst (Pt/C). The outstanding ORR performance can be attributed to the synergetic effect of the N-content functional group, the Co nanoparticles, and the carbon framework. Furthermore, an Al-air battery was assembled with a Co and N co-doped biocarbon electrocatalyst as an air cathode, which achieved high power density (32.24 mW cm^{-2}) and excellent energy storage performance, indicating the Co and N co-doped biocarbon catalyst could easily be utilized as an efficient electrocatalyst in the Al-air battery.

2. Results and Discussion

2.1. Morphological and Structural Characterization

The morphology of as-prepared catalysts was first characterized by SEM and TEM. As shown in Figure 1a and Figure S1, a large number of pores are randomly distributed in the carbon skeleton of NC and CoNC. Furthermore, numerous particles are distributed in and on the skeleton of CoNC. In the TEM image shown in Figure 1b, several nanoparticles ranging from 15 nm to 40 nm can be observed in CoNC. From HR-TEM in Figure 1c, these nanoparticles are encapsulated in the CoNC skeleton and possess lattice spacing of 0.212 nm corresponding to Co particles. Raman spectra were applied to assess the defects of as-prepared materials. As shown in Figure 1d, Raman spectra of the NC and CoNC both have two obvious peaks (denoted as D band and G band) located in 1350 cm^{-1} and 1590 cm^{-1}, which correspond to local defects of carbon materials and graphite degree graphitic in-plane vibration of the carbon materials, respectively. The intensity ratio of D band and G band (I_D/I_G) indicates the defect degree of carbon materials. The I_D/I_G of the CoNC and NC is about 1.06 and 0.95, respectively, which suggests that the CoNC materials contain more defects in the carbon skeleton than those of NC. Subsequently, the difference in morphology was further discussed via a nitrogen adsorption-desorption measurement. Based on nitrogen adsorption-desorption isotherms (Figure 1e), it can be noted that the CoNC possessed higher specific surface areas (~165 m^2 g^{-1}) than that of NC (~106 m^2 g^{-1}). Likewise, the CoNC also showed the lowest average pore size (2.99 nm), lower than that of NC (5.47 nm) (Figure 1f). The possible reason for the above phenomenon might be

ascribed to the sharp shrinking of the carbon matrix and catalytic effect induced by transition metal during the pyrolysis process [35,36].

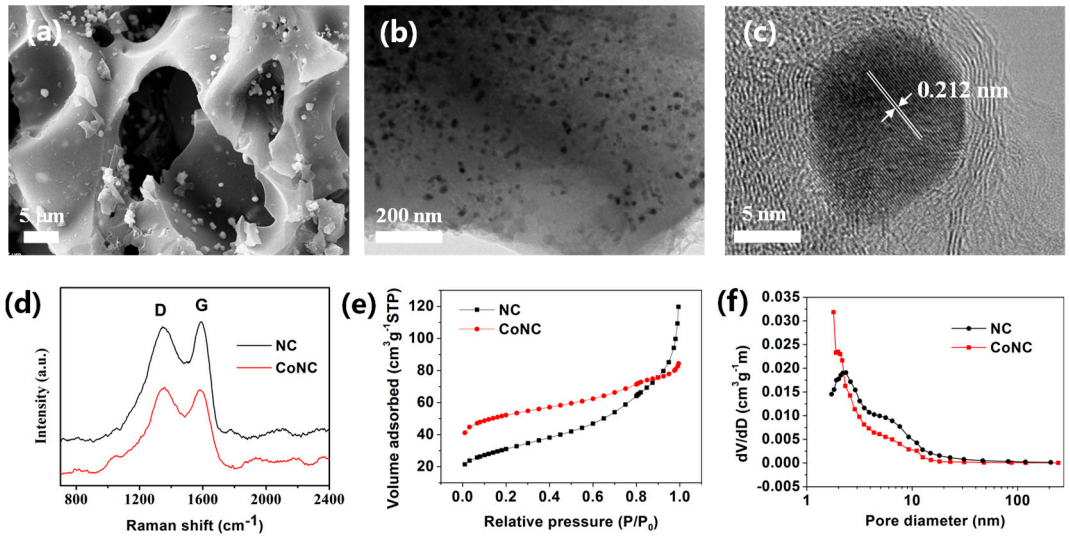

Figure 1. The SEM and TEM images of cobalt nitrogen co-doped carbon material (CoNC) (**a**–**c**). Raman spectra (**d**), N_2 adsorption/desorption isotherms (**e**) and the corresponding pore size (**f**).

The chemical states of as-prepared catalysts were studied by X-ray photoelectron spectroscopy (XPS). As shown in Figure 2a, the spectrum of CoNC contains four significant peaks with locations at 285 eV, 533 eV, 400 eV, and 782 eV corresponding to the C, O, N, Co elements, respectively. These results corresponded to the observation of the SEM and TEM images, suggesting that there are Co particles in CoNC. In a high-resolution C1s spectra of CoNC (Figure 2b), the detected peaks can be deconvoluted into 284.6 eV, 286.4 eV, 289.1 eV, and 285.4 eV, and each of them indicates the existence of C-C bond, C=O bond, O-C=O, and C-N bond in CoNC, respectively. Among these element peaks, the existence of a C-N bond implies the successful doping of N elements into the carbon skeleton. Subsequently, the types of N doped in carbon materials can be studied by high-resolution N1s spectra. As shown in Figure 2c, the N1s spectra can be fitted well with 398.4 eV, 399.2 eV, and 402.2 eV, which represent pyridinic-N, pyrrolic-N, and graphitic-N, respectively. It should be noted that the pyridinic-N is the first place where carbon-based ORR catalyst absorbs O_2 and starts the ORR [37–40]. Meanwhile, the graphitic-N can become the electron-donor and facilitate charge mobility. As shown in Figure 2c and Figure S2, the CoNC material has a higher proportion of pyridinic-N and graphitic-N in N species than that of the NC material, which could further suggest that the CoNC is able to provide more efficient ORR performance than the NC.

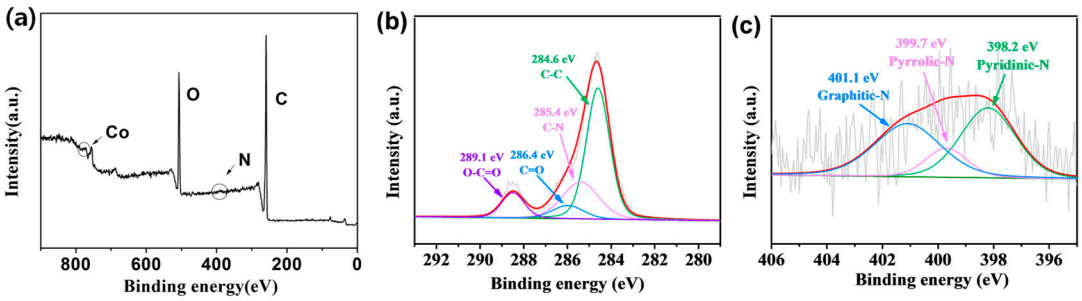

Figure 2. X-ray photoelectron spectroscopy (XPS) survey spectrum of CoNC (**a**), C1s and N1s XPS spectrum of CoNC (**b**,**c**).

2.2. Electrocatalytic Characteristics and Active Sites

The electrocatalytic activities of the four as-prepared samples were first investigated via cyclic voltammetry (CV) tests performed via an electrochemical workstation (CHI 750e) with three-electrode systems. As shown in Figure 3a and Figure S3, NC and CoNC show obvious redox peaks located at 0.69 V and 0.81 V vs. RHE at O_2-saturated KOH solution, and no obvious redox peak can be observed in CV curves at Ar-saturated KOH solution. This indicates that these redox peaks are formed by the ORR process. The CoNC catalyst possesses the positive ORR redox peak, which is comparable to the redox peak (0.82 V vs. RHE) shown in Pt/C (Figure 3b).

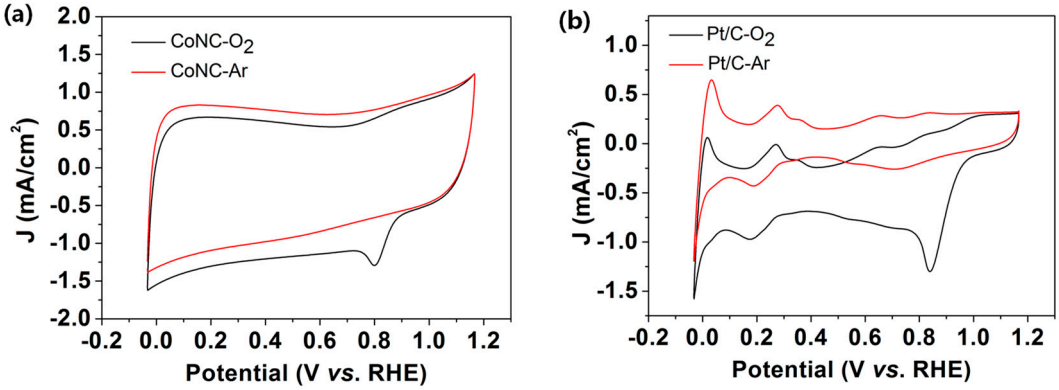

Figure 3. Cyclic voltammetry (CV) curves of CoNC (**a**) and Pt/C (**b**) in O_2- and Ar-saturated 0.1 M KOH solution.

To further study the catalytic activities and ORR kinetics of the as-prepared catalysts, linear sweep voltammetry (LSV) tests were characterized with an rotating disk electrode (RDE) electrode. As shown in corresponding LSV curves (Figure 4a,b, the bar plot corresponds to current density and the line corresponds to onset potential), CoNC shows the higher positive onset potential (0.86V vs. RHE) and limiting current density (4.91 mA cm^{-2}) than the PC (0.78 V, 4.33 mA cm^{-2}) and NC (0.84 V, 4.32 mA cm^{-2}) catalysts. Furthermore, these properties of CoNC are comparable to the benchmark catalyst of Pt/C, for which the onset potential and limiting current density are shown as 0.9 V and 5.67 mA cm^{-2}, respectively.

As numerous works reported, ORR has two major pathways to reduce oxygen into water—the two-electron pathway and the four-electron pathway, respectively. In the four-electron pathway, oxygen is directly reduced to water and is able to provide more positive potential during the ORR process, whereas the two-electron pathway first reduces O_2 to H_2O_2 then further reduces it to water. Thus, in order to investigate the catalytic pathway for CoNC, the ORR kinetics of CoNC were studied with RDE at different rotating speeds ranging from 100 rpm to 2500 rpm (Figure 4c). As shown in Figure 4d, LSV curves combined with the Koutecky-Lecich (K-L) equation are able to obtain several K-L plots at different potentials, which exhibits good parallelism and linearity, suggesting a first-order reaction toward ORR. The calculated electron transfer number is 3.73, which closed to the theoretical value 4, and suggests the four-electron dominant pathway during ORR. Meanwhile, Pt/C also shows the four-electron dominant pathway as electron transfer number (n = 4.03) calculated from K-L plots (Figure S4). For further study in ORR kinetic for CoNC, the rotating ring-disk electrode (RRDE) was used for testing the H_2O_2 productivity and electron transfer numbers while catalyzing ORR. As shown in Figure S5, CoNC produces a low proportion of H_2O_2 (less than 11.8%) and high electron transfer numbers (about 3.84) when ORR is carried out, while Pt/C shows 5.4% of H_2O_2 productivity and a 4.02 electron transfer number. These results elaborate that CoNC possesses the remarkable ORR catalytic activities in alkaline media and has the potential to be applied in metal-air batteries. The long-time durability tests were carried out by chronoamperometry measurement at 900 rpm in O_2-saturated 0.l M KOH. As shown in Figure S6, after a 15000 s long-time durability test, the CoNC is

still able to provide 94.82% of initial current density, while the Pt/C can only maintain 76.64% of initial current density. This indicates that CoNC holds excellent long-term durability, which further benefits the stability of batteries assembled with CoNC.

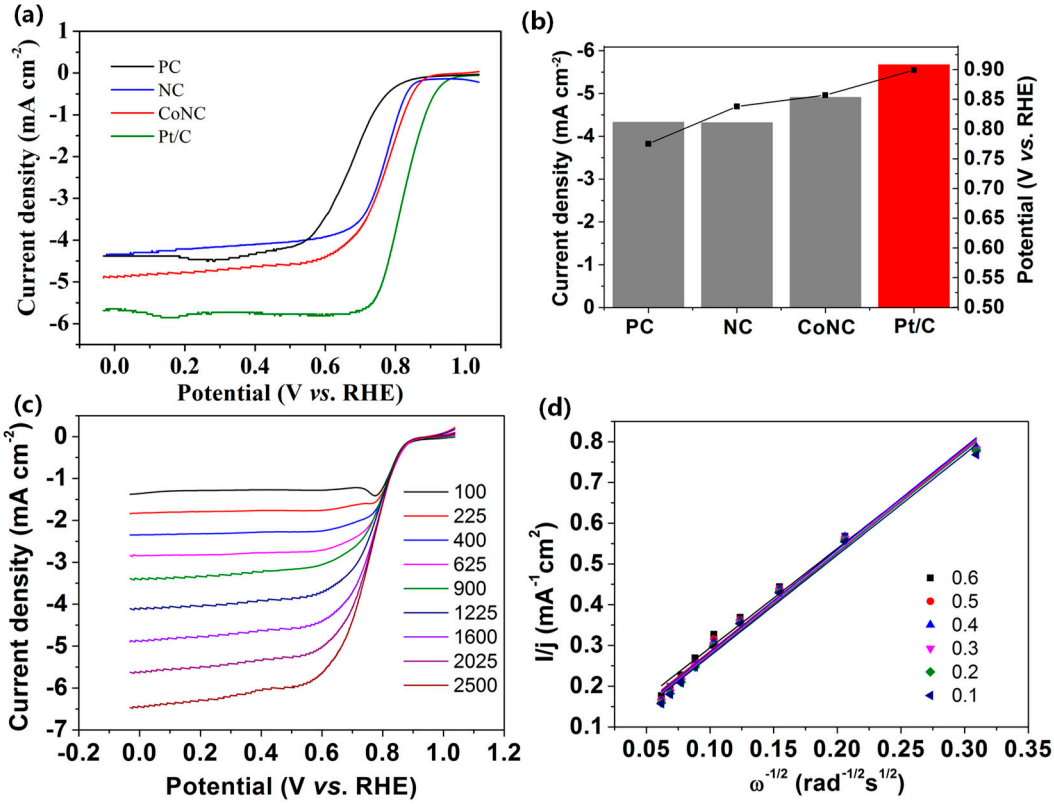

Figure 4. The linear sweep voltammetry (LSV) curves of PC, NC, CoNC and Pt/C catalysts at 1600 rpm (**a**).The onset potentials and limiting current density of catalysts (**b**).The LSV curves of CoNC catalyst at the rotation speeds of 100, 225, 400, 625, 900, 1225, 1600, 2025 and 2500 rpm (**c**). The corresponding Koutecky-Levich (K-L) plots (**d**).

Subsequently, the home-built Al-air batteries were assembled with CoNC and Pt/C in order to demonstrate the practical application performance of catalysts. As shown in Figure 5a, the polarization curves of Al-air batteries were first used for estimating the capability of Al-air batteries. The corresponding power density calculated from the polarization curve of CoNC shows that the maximum power density it can provide is 32.24 mW cm^{-2}, while the maximum power density for Al-air batteries assembled with Pt/C is 43.70 mW cm^{-2}. The electrochemical impedance spectroscopy (EIS) was used to analyze the resistance in Al-air batteries. As calculated by the Nyquist plots in Figure S7, the internal resistance of the Al-air battery with CoNC is 3.46 Ω, which is comparable to that of the battery with 20 wt% Pt/C (3.29 Ω). In order to assess the long-term working property of the battery, the galvanostatic discharge performance was tested in a constant current of 20 mA cm^{-2} (Figure 5b). After a 5000 s test, the voltages of batteries with CoNC and Pt/C decreased 0.04 V and 0.21 V, respectively, and the voltages of batteries with CoNC remained at the constant discharge voltage of 1.17 V at 20 mA cm^{-2}. The superior durability of batteries assembled with CoNC can be attributed to the excellent catalytic durability of CoNC.

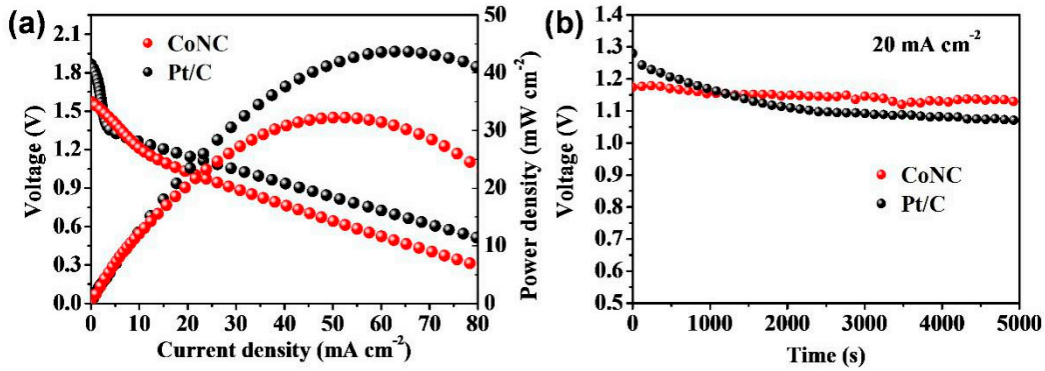

Figure 5. The polarization curves and corresponding power densities of the Al-air batteries with two catalysts (**a**). The galvanostatic discharge curves of Al-air batteries with two catalysts at the constant current density of 20 mA cm^{-2} (**b**).

3. Experimental Section

3.1. Preparation of Co and N Co-Doped Biocarbon

The Co and N co-doped biocarbon is synthesized by a one-step pyrolysis method. Specifically, a mixture of chitin (2 g, MYM biological technology company limited, Nanjing, China), $CoCl_2 \cdot H_2O$ (0.6 g, Fuchen chemical reagents factory, Tianjin, China) and urea (2 g, Beijing Chemical Works, Beijing, China) were ground thoroughly and dissolved into 40 mL of deionized water. Then the mixture was stirred overnight with a string speed of 600 rpm to form a homogeneous solution that was then dried at 60 °C for 48 h. Subsequently, the resulting sample was pyrolyzed at 800 °C for 1 h at a heating rate of 5 °C min^{-1} (Sager SG-GS1700). The resultant powder, N and Co co-doped biocarbon material, was denoted as CoNC. As controls, directly carbonized chitin (PC) and N-doped bio-carbon (NC) without any Co, were also prepared by the same method. For comparison, 20 wt% Pt/C was prepared and the loading for Pt was about 20 μg cm^{-2}.

3.2. Physicochemical Characterization

The morphologies of as-prepared catalysts were studied by scanning electron microscopy (SEM) with a JEOL JSM-7500F field emission scanning electron microscope and transmission electron microscope (TEM) with a JEOL-2010 electron microscope operating at 200 kV. X-ray photoelectron spectroscopy (XPS) was performed on ESCALAB 250Xi (Thermo Scientific, Shanghai, China). A laser microscope system (B&W TEK BTC 162E) with an exciting laser of 532 nm was applied to study the Raman shifts. Then, the specific surface area and pore size were studied via automated gas sorption analyzer (ASAP 2020M-Physisoprtion Analyzer, Changchun, China) at 77 K. The Brunauer–Emmett–Teller method was used to calculate the specific surface area and the pore size.

3.3. Electrochemical Measurements

The electrochemical measurements were carried on a CHI 750E electrochemical workstation system with a typical three-electrode cell in 0.1 M KOH solution at room temperature. Glassy carbon electrode, Ag/AgCl, and Pt wire were used as a working electrode, reference electrode, and counter electrode, respectively. The catalyst inks were prepared by ultrasonically dispersing 5 mg of as-prepared catalysts, 5 mg of carbon black, and 50 μL of Nafion in 1 mL of ethanol. Then, 20 μL well-dispersed catalyst inks were loaded on a working electrode (5.5 mm diameter), leading to a 100 μg cm^{-2} catalyst loading. The as-prepared electrodes were dried completely at room temperature before the electrochemical tests. Cyclic voltammetry (CV) was measured in O_2- and Ar-saturated 0.1 M KOH electrolyte with a scan rate of 10 mV s^{-1}. For the ORR kinetics study, the linear sweep voltammetry (LSV) tests were

performed at rotating rates from 100 to 2500 in O_2-saturated electrolyte with a scan speed of 10 mV s^{-1}. The long-time durability of catalysts was tested in O_2-saturated 0.1 M KOH by chronoamperometry.

The electrons transfer number during ORR was analyzed from RDE measurements by using the following Koutecky-Lecich (K-L) equations (Equations (1) and (2)):

$$j^{-1} = {j_K}^{-1} + {j_L}^{-1} = {j_K}^{-1} + B^{-1}\omega^{-1/2} \quad (1)$$

$$\mathrm{B} = 0.2\mathrm{FC_0}(\mathrm{D_0})^{2/3}v^{-1/6} \quad (2)$$

where j_L and j_K are the limiting current for the electrode reaction of reactive species by the diffusion-controlled process and the kinetic current, respectively. F (96486.4 C mol^{-1}) is the Faraday constant, n is the electron transfer number, C_0* (1.2×10^{-6} mol cm^{-3}) is the concentration of O_2 in 0.1 M KOH solution, D_0 (1.9×10^{-5} cm^2 s^{-1}) is the diffusion coefficient of O_2 in 0.1 M KOH, ω (rad s^{-1}) is rotation rate and v (0.01 cm^2 s^{-1}) is the kinematic viscosity of the electrolyte [41,42].

3.4. Al-Air Battery Tests

The measurements of Al-air batteries were tested via home-built electrochemical cells. Al plate (99% purity) and 6 M KOH aqueous solution were used as the anode and electrolyte, respectively. A cathode was prepared by catalyst layer, carbon cloth (middle layer), carbon-based layer, and the diffusion layer. The mixture of carbon black and 40% Polytetrafluoroethylene (PTFE) was coated onto carbon cloth to form a carbon-based layer that prevents penetration of PTFE in the following process. A diffusion layer was prepared by applying a 60% PTFE layer coating on the carbon-based layer and heating it at 370 °C for 20 min. Subsequently, a catalyst layer was prepared by loading a mixture of CoNC, 5% Nafion, and ethanol on the other side of the carbon cloth (25 mg cm^{-2}). For comparison, the Al-air battery that used commercial Pt/C as an air cathode was fabricated via the same procedures. The polarization curves and long-term discharge performances were tested by electrochemical workstation (CHI 750E) under air atmosphere.

4. Conclusions

In conclusion, a low-cost method was developed to synthesize efficient ORR catalyst derived from chitin. The biomass-derived electrocatalyst (CoNC) possesses high specific surface area, which contributes to enhanced ORR performance, and shows good ORR catalytic activities during ORR in alkaline media. In addition, Al-air batteries equipped with CoNC electrocatalyst show good power density and excellent long-term discharging durability, which is attributed to the efficient catalytic activities of CoNC. This work paves a new way for mass production of low-cost ORR catalyst and the utilization of biomass product.

Supplementary Materials: The following are available online at http://www.mdpi.com/2073-4344/9/11/954/s1, Figure S1: The SEM and TEM images of NC, Figure S2: N1s XPS spectrum of NC, Figure S3: CV curves of NC catalysts, Figure S4: The LSV curves of Pt/C catalyst at the rotation speeds of 100, 225, 400, 625, 900, 1225, 1600, 2025 and 2500 rpm (a). The corresponding Koutecky-Levich (K-L) plots (b), Figure S5: The H_2O_2 yield and n value of CoNC and Pt/C, Figure S6: The i-t chronoamperometric curves of CoNC and Pt/C for 15000 s in an O_2-saturated 0.1 M KOH solution, Figure S7: Nyquist plots of CoNC and commercial Pt/C from 100 KHz to 0.01 Hz.

Author Contributions: G.L. and S.Y. designed experiments; M.W. and J.M. carried out experiments; M.W. and Z.C. analyzed sequencing data; M.W. and H.Y. wrote the manuscript.

Funding: This work was funded by the National Natural Science Foundation of China (grant number: 51605188, 51605187), Department of Education of Jilin Province (grant number: JJKH20180093KJ, JJKH20181163KJ), and Jilin Provincial Science & Technology Department (Grant Number: 20180201004GX).

Conflicts of Interest: The author declares that there is no conflict of interests regarding the publication of this article.

References

1. Liu, Z.N.; Li, Z.Y.; Ma, J.; Dong, X.; Ku, W.; Wang, M.; Sun, H.; Liang, S.; Lu, G.L. Nitrogen and cobalt-doped porous biocarbon materials derived from corn stover as efficient electrocatalysts for aluminum-air batteries. *Energy* **2018**, *162*, 453–459. [CrossRef]
2. Guo, Z.Y.; Li, C.; Liu, J.Y.; Wang, Y.G.; Xia, Y.Y. A Long-Life Lithium-Air Battery in Ambient Air with a Polymer Electrolyte Containing a Redox Mediator. *Angew. Chem. Int. Ed.* **2017**, *56*, 7505–7509. [CrossRef] [PubMed]
3. Pan, J.; Xu, Y.Y.; Yang, H.; Dong, Z.; Liu, H.; Xia, B.Y. Advanced Architectures and Relatives of Air Electrodes in Zn-Air Batteries. *Adv. Sci. (Weinh.)* **2018**, *5*, 1700691. [CrossRef] [PubMed]
4. Ryu, J.; Park, M.; Cho, J. Advanced Technologies for High-Energy Aluminum-Air Batteries. *Adv. Mater.* **2019**, *31*, 1804784. [CrossRef] [PubMed]
5. Li, J.Z.; Chen, M.J.; Cullen, D.A.; Hwang, S.; Wang, M.Y.; Li, B.Y.; Liu, K.X.; Karakalos, S.; Lucero, M.; Zhang, H.G.; et al. Atomically dispersed manganese catalysts for oxygen reduction in proton-exchange membrane fuel cells. *Nat. Catal.* **2018**, *1*, 935–945. [CrossRef]
6. Yang, D.J.; Zhang, L.J.; Yan, X.C.; Yao, X.D. Recent Progress in Oxygen Electrocatalysts for Zinc-Air Batteries. *Small Methods* **2017**, *1*, 1700209. [CrossRef]
7. Liu, Y.; Liu, Z.; Liu, H.; Liao, M. Novel Porous Nitrogen Doped Graphene/Carbon Black Composites as Efficient Oxygen Reduction Reaction Electrocatalyst for Power Generation in Microbial Fuel Cell. *Nanomaterials* **2019**, *9*, 836. [CrossRef]
8. Liu, J.; Jiao, M.G.; Lu, L.L.; Barkholtz, H.M.; Li, Y.P.; Wang, Y.; Jiang, L.H.; Wu, Z.J.; Liu, D.J.; Zhuang, L.; et al. High performance platinum single atom electrocatalyst for oxygen reduction reaction. *Nat. Commun.* **2017**, *8*, 15938. [CrossRef]
9. Liu, H.Y.; Qin, J.Q.; Zhao, S.Q.; Gao, Z.M.; Fu, Q.; Song, Y.J. Two-dimensional circular platinum nanodendrites toward efficient oxygen reduction reaction and methanol oxidation reaction. *Electrochem. Commun.* **2019**, *98*, 53–57. [CrossRef]
10. Li, Y.; Xia, X.H. Study on the Mechanism and Kinetics of Oxygen Reduction Reaction on 3D Porous Platinum Film Constructed Using Colloidal Crystal Template. *J. Nanosci. Nanotech.* **2016**, *16*, 12388–12393. [CrossRef]
11. Lange, K.; Schulz-Ruhtenberg, M.; Caro, J. Platinum Electrodes for Oxygen Reduction Catalysis Designed by Ultrashort Pulse Laser Structuring. *Chemelectrochem* **2017**, *4*, 570–576. [CrossRef]
12. Oh, T.; Kim, K.; Kim, J. Controllable active sites and facile synthesis of cobalt nanoparticle embedded in nitrogen and sulfur co-doped carbon nanotubes as efficient bifunctional electrocatalysts for oxygen reduction and evolution reactions. *J. Energy Chem.* **2019**, *38*, 60–67. [CrossRef]
13. Kang, Y.S.; Choi, D.; Park, H.-Y.; Yoo, S.J. Tuning the surface structure of PtCo nanocatalysts with high activity and stability toward oxygen reduction. *J. Ind. Eng. Chem.* **2019**, *78*, 448–454. [CrossRef]
14. Kim, S.; Kato, S.; Ishizaki, T.; Li, O.L.; Kang, J. Transition Metal (Fe, Co, Ni) Nanoparticles on Selective Amino-N-Doped Carbon as High-Performance Oxygen Reduction Reaction Electrocatalyst. *Nanomaterials* **2019**, *9*, 742. [CrossRef] [PubMed]
15. Zhang, B.; Xiao, C.H.; Xiang, Y.; Dong, B.T.; Ding, S.J.; Tang, Y.H. Nitrogen-Doped Graphene Quantum Dots Anchored on Thermally Reduced Graphene Oxide as an Electrocatalyst for the Oxygen Reduction Reaction. *Chemelectrochem* **2016**, *3*, 864–870. [CrossRef]
16. Su, C.Y.; Cheng, H.; Li, W.; Liu, Z.Q.; Li, N.; Hou, Z.F.; Bai, F.Q.; Zhang, H.X.; Ma, T.Y. Atomic Modulation of FeCo-Nitrogen-Carbon Bifunctional Oxygen Electrodes for Rechargeable and Flexible All-Solid-State Zinc-Air Battery. *Adv. Energy Mater.* **2017**, *7*, 1602242. [CrossRef]
17. Zhu, J.W.; Li, W.Q.; Li, S.H.; Zhang, J.; Zhou, H.; Zhang, C.T.; Zhang, J.A.; Mu, S.C. Defective N/S-Codoped 3D Cheese-Like Porous Carbon Nanomaterial toward Efficient Oxygen Reduction and Zn-Air Batteries. *Small* **2018**, *14*, 1800563. [CrossRef]
18. Ma, Z.; Wang, K.X.; Qiu, Y.F.; Liu, X.Z.; Cao, C.Y.; Feng, Y.J.; Hu, P.A. Nitrogen and sulfur co-doped porous carbon derived from bio-waste as a promising electrocatalyst for zinc-air battery. *Energy* **2018**, *143*, 43–55. [CrossRef]
19. Wang, G.H.; Deng, Y.J.; Yu, J.N.; Zheng, L.; Du, L.; Song, H.Y.; Liao, S.J. From Chlorella to Nestlike Framework Constructed with Doped Carbon Nanotubes: A Biomass-Derived, High-Performance, Bifunctional Oxygen Reduction/Evolution Catalyst. *ACS Appl. Mater. Interface* **2017**, *9*, 32168–32178. [CrossRef]

20. Zhang, Z.P.; Gao, X.J.; Dou, M.L.; Ji, J.; Wang, F. Biomass Derived N-Doped Porous Carbon Supported Single Fe Atoms as Superior Electrocatalysts for Oxygen Reduction. *Small* **2017**, *13*, 1604290. [CrossRef]
21. Xu, L.N.; Fan, H.; Huang, L.X.; Xia, J.L.; Li, S.H.; Li, M.; Ding, H.Y.; Huang, K. Chrysanthemum-derived N and S co-doped porous carbon for efficient oxygen reduction reaction and aluminum-air battery. *Electrochim. Acta* **2017**, *239*, 1–9. [CrossRef]
22. Liu, L.; Yang, X.F.; Ma, N.; Liu, H.T.; Xia, Y.Z.; Chen, C.M.; Yang, D.J.; Yao, X.D. Scalable and Cost-Effective Synthesis of Highly Efficient Fe2N-Based Oxygen Reduction Catalyst Derived from Seaweed Biomass. *Small* **2016**, *12*, 1295–1301. [CrossRef] [PubMed]
23. Lu, G.; Zhu, Y.; Lu, L.; Xu, K.; Wang, H.; Jin, Y.; Ren, Z.J.; Liu, Z.; Zhang, W. Iron-rich nanoparticle encapsulated, nitrogen doped porous carbon materials as efficient cathode electrocatalyst for microbial fuel cells. *J. Power Sources* **2016**, *315*, 302–307. [CrossRef]
24. Lu, G.; Zhu, Y.; Xu, K.; Jin, Y.; Ren, Z.J.; Liu, Z.; Zhang, W. Metallated porphyrin based porous organic polymers as efficient electrocatalysts. *Nanoscale* **2015**, *7*, 18271–18277. [CrossRef]
25. Yan, L.; Yu, J.; Houston, J.; Flores, N.; Luo, H. Biomass Derived Porous Nitrogen doped Carbon for Electrochemical Devices. *Green Energy Environ.* **2017**, *2*, 84–99. [CrossRef]
26. Li, Y.H.; Liu, D.B.; Gan, J.; Duan, X.Z.; Zang, K.T.; Ronning, M.; Song, L.; Luo, J.; Chen, D. Sustainable and Atomically Dispersed Iron Electrocatalysts Derived from Nitrogen- and Phosphorus-Modified Woody Biomass for Efficient Oxygen Reduction. *Adv. Mater. Interfaces* **2019**, *6*, 1801623. [CrossRef]
27. Wu, D.Y.; Zhu, C.; Shi, Y.T.; Jing, H.Y.; Hu, J.W.; Song, X.D.; Si, D.H.; Liang, S.X.; Hao, C. Biomass-Derived Multilayer-Graphene-Encapsulated Cobalt Nanoparticles as Efficient Electrocatalyst for Versatile Renewable Energy Applications. *ACS Sustain. Chem. Eng.* **2019**, *7*, 1137–1145. [CrossRef]
28. Wei, Q.L.; Yang, X.H.; Zhang, G.X.; Wang, D.N.; Zuin, L.; Banham, D.; Yang, L.J.; Ye, S.Y.; Wang, Y.L.; Mohamedi, M.; et al. An active and robust Si-Fe/N/C catalyst derived from waste reed for oxygen reduction. *Appl. Catal. B Environ.* **2018**, *237*, 85–93. [CrossRef]
29. Yuan, H.; Deng, L.; Cai, X.; Zhou, S.; Chen, Y.; Yuan, Y. Nitrogen-doped carbon sheets derived from chitin as non-metal bifunctional electrocatalysts for oxygen reduction and evolution. *RSC Adv.* **2015**, *5*, 56121–56129. [CrossRef]
30. Bo, W.; Li, S.; Wu, X.; Liu, J.; Jing, C. Biomass chitin-derived honeycomb-like nitrogen-doped carbon/graphene nanosheet networks for applications in efficient oxygen reduction and robust lithium storage. *J. Mater. Chem. A* **2016**, *4*. [CrossRef]
31. Chen, J.; Qiu, L.; Li, Z.; Gao, G.; Zhong, W.; Zhang, P.; Gong, Y.; Deng, L. Chitin-derived porous carbon loaded with Co, N and S with enhanced performance towards electrocatalytic oxygen reduction, oxygen evolution, and hydrogen evolution reactions. *Electrochim. Acta* **2019**, *304*, 350–359. [CrossRef]
32. Borghei, M.; Laocharoen, N.; Kibena-Poldsepp, E.; Johansson, L.S.; Campbell, J.; Kauppinen, E.; Tammeveski, K.; Rojas, O.J. Porous N,P-doped carbon from coconut shells with high electrocatalytic activity for oxygen reduction: Alternative to Pt-C for alkaline fuel cells. *Appl. Catal. B Environ.* **2017**, *204*, 394–402. [CrossRef]
33. Jiang, Z.Q.; Zhao, X.S.; Tian, X.N.; Luo, L.J.; Fang, J.H.; Gao, H.Q.; Jiang, Z.J. Hydrothermal Synthesis of Boron and Nitrogen Codoped Hollow Graphene Microspheres with Enhanced Electrocatalytic Activity for Oxygen Reduction Reaction. *ACS Appl. Mater. Interface* **2015**, *7*, 19398–19407. [CrossRef] [PubMed]
34. Meng, F.L.; Zhong, H.X.; Bao, D.; Yan, J.M.; Zhang, X.B. In Situ Coupling of Strung Co4N and Intertwined N-C Fibers toward Free-Standing Bifunctional Cathode for Robust, Efficient, and Flexible Zn Air-Batteries. *J. Am. Chem. Soc.* **2016**, *138*, 10226–10231. [CrossRef] [PubMed]
35. Chen, Z.; Gao, X.; Wei, X.; Wang, X.; Li, Y.; Wu, T.; Guo, J.; Gu, Q.; Wu, W.D.; Chen, X.D. Directly anchoring Fe 3 C nanoclusters and FeN x sites in ordered mesoporous nitrogen-doped graphitic carbons to boost electrocatalytic oxygen reduction. *Carbon* **2017**, *121*, 143–153. [CrossRef]
36. Li, C.L.; Wu, M.C.; Liu, R. High-performance bifunctional oxygen electrocatalysts for zinc-air batteries over mesoporous Fe/Co-N-C nanofibers with embedding FeCo alloy nanoparticles. *Appl. Catal. B Environ.* **2019**, *244*, 150–158. [CrossRef]
37. Liu, Z.; Li, Z.; Tian, S.; Wang, M.; Sun, H.; Liang, S.; Chang, Z.; Lu, G. Conversion of peanut biomass into electrocatalysts with vitamin B12 for oxygen reduction reaction in Zn-air battery. *Int. J. Hydrogen Energy* **2019**, *44*, 11788–11796. [CrossRef]

38. Wang, Y.; Zhu, M.; Wang, G.; Dai, B.; Yu, F.; Tian, Z.; Guo, X. Enhanced Oxygen Reduction Reaction by In Situ Anchoring Fe_2N Nanoparticles on Nitrogen-Doped Pomelo Peel-Derived Carbon. *Nanomaterials* **2017**, *7*, 404. [CrossRef]
39. Lu, G.; Li, Z.; Fan, W.; Wang, M.; Yang, S.; Li, J.; Chang, Z.; Sun, H.; Liang, S.; Liu, Z. Sponge-like N-doped carbon materials with Co-based nanoparticles derived from biomass as highly efficient electrocatalysts for the oxygen reduction reaction in alkaline media. *RSC Adv.* **2019**, *9*, 4843–4848. [CrossRef]
40. Lu, J.; Zeng, Y.; Ma, X.; Wang, H.; Gao, L.; Zhong, H.; Meng, Q. Cobalt Nanoparticles Embedded into N-Doped Carbon from Metal Organic Frameworks as Highly Active Electrocatalyst for Oxygen Evolution Reaction. *Polymers* **2019**, *11*, 828. [CrossRef]
41. Stosevski, I.; Krstic, J.; Milikic, J.; Sljukic, B.; Kacarevic-Popovic, Z.; Mentus, S.; Miljanic, S. Radiolitically synthesized nano Ag/C catalysts for oxygen reduction and borohydride oxidation reactions in alkaline media, for potential applications in fuel cells. *Energy* **2016**, *101*, 79–90. [CrossRef]
42. Zhang, J.W.; Xu, D.; Wang, C.C.; Guo, J.N.; Yan, F. Rational Design of Fe1-xS/Fe3O4/Nitrogen and Sulfur-Doped Porous Carbon with Enhanced Oxygen Reduction Reaction Catalytic Activity. *Adv. Mater. Interfaces* **2018**, *5*, 1701461.